Wall effects on Reiner-Rivlin liquid spheroid

B. R. Jaiswal[a,*], B. R. Gupta[a]

[a]*Department of Mathematics, Jaypee University of Engineering and Technology, 473226 Guna, M. P., India*

Abstract

An analysis is carried out to study the flow characteristics of creeping motion of an inner non-Newtonian Reiner-Rivlin liquid spheroid $r = 1 + \sum_{k=2}^{\infty} \alpha_k G_k(\cos\theta)$, here α_k is very small shape factor and G_k is Gegenbauer function of first kind of order k, at the instant it passes the centre of a rigid spherical container filled with a Newtonian fluid. The shape of the liquid spheroid is assumed to depart a bit at its surface from the shape a sphere. The analytical expression for stream function solution for the flow in spherical container is obtained by using Stokes equation. While for the flow inside the Reiner-Rivlin liquid spheroid, the expression for stream function is obtained by expressing it in a power series of S, characterizing the cross-viscosity of Reiner-Rivlin fluid. Both the flow fields are then determined explicitly by matching the boundary conditions at the interface of Newtonian fluid and non-Newtonian fluid and also the condition of impenetrability and no-slip on the outer surface to the first order in the small parameter ϵ, characterizing the deformation of the liquid sphere. As an application, we consider an oblate liquid spheroid $r = 1 + 2\epsilon G_2(\cos\theta)$ and the drag and wall effects on the body are evaluated. Their variations with regard to separation parameter, viscosity ratio λ, cross-viscosity, i.e., S and deformation parameter ϵ are studied and demonstrated graphically. Several well-noted cases of interest are derived from the present analysis. Attempts are made to compare between Newtonian and Reiner-Rivlin fluids which yield that the cross-viscosity μ_c is to decrease the wall effects K and to increase the drag D_N when deformation is comparatively small. It is observed that drag not only varies with λ, but as η increases, the rate of change in behavior of drag force increases also.
© 2014 University of West Bohemia. All rights reserved.

Keywords: Reiner-Rivlin fluid, Gegenbauer function, stream functions, liquid spheroid, drag force, wall correction factor, spherical container

1. Introduction

Since the pioneering work [31], a considerable body of knowledge has accrued on the drag force experienced by a range of shapes of particles settling in immovable fluid media or held stationary in moving fluids. A spherical particle is unique in that it presents the same projected area to the oncoming fluid irrespective of its orientation. For nonspherical particles, on the other hand, the orientation must be known before their terminal settling velocity or the drag force acting on them can be calculated. On the contrary, under appropriate circumstances, non-spherical particles are vulnerable to accomplish a preferred or most stable orientation irrespective of their preliminary orientation. These entire phenomenons are strongly influenced not only by the shape of the particle, its size and density, fluid properties, but also by the shape and size of confining boundaries and the fluid motion as well. The literature, not as much extensive as that of spherical particles, available on regularly or irregularly shaped nonspherical particles in incompressible Newtonian and non-Newtonian fluid media has been reviewed by few researchers in the recent past. Ramkissoon, independently, examined the problems of symmetrical flow of Newtonian fluid past a Newtonian fluid spheroid [22] and non-Newtonian Reiner-Rivlin fluid

---

*Corresponding author. Tel.: +91 82 25 892 602, e-mail: jaiswal.bharat@gmail.com.

spheroid [19] and evaluated drag on these fluid bodies. The problems of Stokes flow of a micropolar fluid past a Newtonian fluid spheroid by [15], a Reiner-Rivlin fluid sphere with no-spin condition for micro rotations by [20] and later this problem was reinvestigated with spin condition for micro rotations by [6]. The paper [5] solved the problem for the case of an approximate sphere in micropolar fluid. The problem of a viscous incompressible fluid past a spheroid which departs but little in shape from a sphere with mixed slip-stick boundary conditions was investigated by [14] and drag exerted on oblate spheroid is calculated which is found in the present case to be less than that of the Stokes resistance for a slightly oblate spheroid.

The problems of motion of a particle at the instant it passes the center of the spherical container serves as a model of interaction in multi-particle systems. The simplest geometry permits one to study the impressive and effective shape of fluid particles on their settling velocity and the drag resistance on approximate sphere. This class of problems is important because it provides some information on wall effects. Wall effects for a sphere at the instant it passes the center of the spherical container have been studied by several investigators and these investigations were abbreviated and summarized by [4, 10, 13] and [7]. A survey of literature regarding the fluid flows past a solid or a liquid body of different shapes indicates that while abundant information is available for flows in an infinite expanse of fluid, but very few studies of wall effects for approximate spheres are available for flows in enclosures. The authors of [2] and [32], independently, considered the motion of a solid sphere in a spherical container and presented the solutions for the case of inner solid sphere. [3] have made an equivalent or analogous study for the motion of an inner classical fluid sphere. The paper [16] investigated the motion of inner Reiner-Rivlin (non-Newtonian) fluid sphere in a spherical container and they deduced that cross viscosity μ_c is to reduce the wall effects. Two years later, [17] also investigated the problem of a solid spherical particle in a spheroidal container. They obtained the expression for the drag on the inner sphere and examined the wall effects and concluded that as the deformation of the spheroidal container increases the wall effects also increase. In all the above mentioned problems, the authors utilized no-slip condition on the surface of the inner sphere. [18] studied the motion of solid spheroidal particle in a spherical container using a slip condition at the surface of the inner particle and evaluated the expression for drag on it and examined the wall effects. They concluded that the wall effects increase as the spheroidal particle becomes more spheroidal. Maul and Kim [11, 12] investigated a point force in a fluid domain bounded by a rigid spherical container and the image of a point force in a spherical container and its connection to the Lorentz reflection formula by using Stokes equation. By applying the boundary conditions of continuity of the velocity, pressure and tangential stresses at the porous-liquid interface, the quasisteady translation and steady rotation of a spherically symmetric composite particle composed of a solid core and a surrounding porous shell located at the center of a spherical cavity filled with an incompressible Newtonian fluid is studied by [8]. The quasisteady translation and steady rotation of a spherically symmetric porous shell located at the center of a spherical cavity filled with an incompressible Newtonian fluid is investigated analytically by [9]. They evaluated the hydrodynamic drag force and torque exerted by the fluid on the porous particle and found that the boundary effects of the cavity wall on the creeping motions of a composite sphere can be significant in appropriate situations. The work [30], independently, has studied the motion of a porous sphere in a spherical container using Brinkmans model in the porous region and concluded that the wall correction factor increases and drag coefficient decreases with permeability parameter. The motion of a spheroidal particle at the instant it passes the centre of a spherical envelope filled with a micropolar fluid is investigated by [23] using the slip condition at the surface of the particle. The flow problem of an incom-

pressible axisymmetrical quasisteady translation and steady rotation of a porous spheroid in a concentric spheroidal container is studied analytically by [24]. Srinivasacharya and Prasad have study the problems on the motion of a porous spherical shell in a bounded medium [27], slow steady rotation of a porous sphere in a spherical container [29], steady rotation of a composite sphere in a concentric spherical cavity [28], creeping motion of a porous approximate sphere with an impermeable core in spherical container [26] and axisymmetric motion of a porous approximate sphere in an approximate spherical container [25]. They found that, in all the cases, the wall correction factor increases and drag decreases as the size of the container increases. The outcomes and motivations of these research findings lead us to discuss the present problem which includes some previous results.

In this paper, we consider the creeping motion of a Reiner-Rivlin liquid spheroid in spherical container and the flow considered is axisymmetric in nature. This, we should mention, is an extension of previous works by [16], where the Reiner-Rivlin droplet was assumed to be perfectly spherical, and [19], where Reiner-Rivlin liquid spheroid was considered in an infinite expanse of Newtonian fluid. Here, we assume that the inner sphere is moving with uniform velocity U in the positive z-direction. Both the internal and external flow fields, flows inside the liquid spheroid and within a spherical container, are determined to the first order in the small parameter characterizing the deformation by using the Stokes approximation and expanding the internal stream function in a power series of a dimensionless parameter S. The drag experienced by the inner liquid spheroid is evaluated, and this enables us to examine the wall effects numerically and graphically as well.

2. Mathematical formulation and solution of the problem

We consider a non-Newtonian Reiner-Rivlin liquid spheroid of radius, $r = 1 + \alpha_k G_k$, and to examine the drag force at an instant it passes the center of a large spherical vessel of radius b containing a steady and incompressible Newtonian fluid (liquid region I). The problem of course, is equivalent to the inner liquid spheroid remains at rest while the outer spherical container moves, say, with constant velocity U in the positive z-direction. Further, we assume that the inner flow (liquid region II) is also steady, incompressible and the liquid spheroid to be stationary. A physical model illustrating the problem under consideration is shown in Fig. 1. The
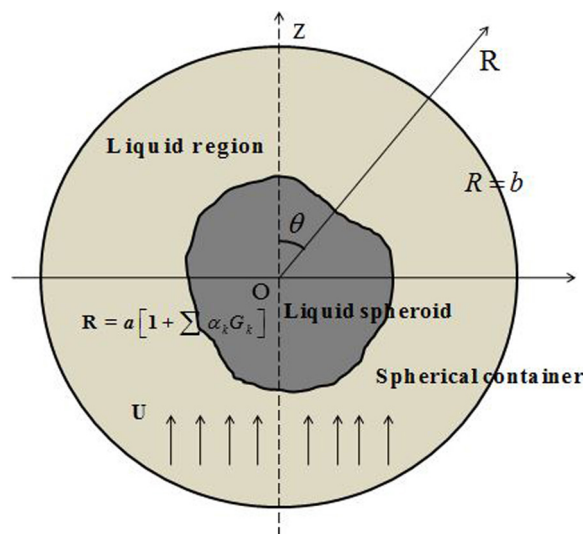

Fig. 1. Physical model and co-ordinate system illustrating the axisymmetric flow past a Reiner-Rivlin liquid spheroid in spherical container

parameters pertaining to the exterior and the interior of the liquid spheroid to be distinguished respectively by the index in the superscripts under the bracket of an entity $\chi^{(i)}$, $i = 1, 2$.

2.1. Basic equations

Within the spherical container (liquid region I), the corresponding flow-field equations describing the motion of a viscous fluid (Newtonian) in region I are governed by the Stokes equation and equation of continuity respectively as

$$\operatorname{grad} \tilde{p}^{(1)} + \mu_1 \operatorname{curlcurl} \tilde{q}^{(1)} = 0 \tag{1}$$

and

$$\operatorname{div} \tilde{q}^{(1)} = 0, \tag{2}$$

where $\tilde{q}^{(1)}$ is the velocity, μ_1 is the coefficient of viscosity and $\tilde{p}^{(1)}$ is the pressure.

The constitutive equation for isotropic non-Newtonian Reiner-Rivlin liquid in the region II takes the form

$$\tilde{\tau}_{ij} = -\tilde{p}^{(2)} \delta_{ij} + 2\mu_2 \tilde{d}_{ij} + \mu_c \tilde{d}_{ik} \tilde{d}_{kj}, \tag{3}$$

where

$$\tilde{d}_{ij} = \frac{1}{2} \left(\tilde{\tilde{q}}^{(2)}_{i,j} + \tilde{\tilde{q}}^{(2)}_{j,i} \right),$$

$\tilde{\tau}_{ij}$ is the stress tensor, $\tilde{d}_{ij}$ is the rate of strain (deformation) tensor, μ_2 is the coefficient of viscosity and μ_c is the coefficient of cross-viscosity of Reiner-Rivlin liquid in region II. The velocity vector and the pressure for region II are respectively denoted by $\tilde{q}^{(2)}$ and $\tilde{p}^{(2)}$.

Let (R, θ, ϕ) denote a spherical polar co-ordinate system with the origin at the center of the sphere of radius a. Since the flow is axially symmetric and the fluid flows in the meridian plane, all the physical quantities are independent of ϕ. Hence, we assume that the velocity vectors $\tilde{q}^{(1)}$ and $\tilde{q}^{(2)}$ can be expressed as

$$\tilde{q}^{(i)} = \tilde{u}_R^{(i)}(R, \theta) \vec{e}_R + \tilde{u}_\theta^{(i)}(R, \theta) \vec{e}_\theta, \quad i = 1, 2. \tag{4}$$

In view of the incompressibility condition $\operatorname{div} \tilde{q}^{(1)} = 0$, we introduce the stream function $\tilde{\psi}^{(i)}(R, \theta) = 0$, $i = 1, 2$ through

$$\tilde{u}_R^{(i)} = \frac{-1}{R^2 \sin \theta} \frac{\partial \tilde{\psi}^{(i)}}{\partial \theta}, \quad \tilde{u}_\theta^{(i)} = \frac{1}{R \sin \theta} \frac{\partial \tilde{\psi}^{(i)}}{\partial R}. \tag{5}$$

In order to non-dimensionalize the values and operators appearing in the governing equations, we insert the following non-dimensional variables:

$$R = ar, \quad \tilde{u}_R = U u_r, \quad \tilde{u}_\theta = U u_\theta, \quad \tilde{\tau}_{ij} = \mu_i \frac{U}{a} \tau_{ij},$$
$$\tilde{d}_{ij} = \frac{U}{a} d_{ij}, \quad \tilde{p} = \mu_i \frac{U}{a} p, \quad \tilde{\psi} = U a^2 \psi,$$

where U and a represent some typical velocity and length of the flow field respectively.

We write the stream function and pressure in the form a power series in S for the internal flow within the liquid spheroid as follows

$$\psi^{(2)} = \psi_0 + \psi_1 S + \psi_2 S^2 + \dots,$$
$$p^{(2)} = p_0 + p_1 S + p_2 S^2 + \dots, \tag{6}$$

where $S = \frac{\mu_c U}{\mu_2 a}$ is the sufficiently small dimensionless number and therefore, the terms in (6) of $O(S > 2)$ can be neglected. The suffixes in (6) represent the zeroth, second and higher order

approximation of the corresponding variables. Following [21], the stream functions ψ_0, ψ_1 and ψ_2 satisfy respectively the following differential equations

$$E^4\psi_0 = 0, \quad E^4\psi_1 = 8r\sin^2\theta\cos\theta, \quad E^4\psi_2 = \frac{32}{3}r^2\sin^2\theta. \tag{7}$$

Particular solutions of the equations mentioned in (7) are respectively given by

$$\psi_0 = (r^4 - r^2)\sin^2\theta, \quad \psi_1 = \frac{2}{21}r^5\sin^2\theta\cos\theta, \quad \psi_2 = \frac{2}{63}r^6\sin^2\theta. \tag{8}$$

Eliminating pressure from (1) and making use of (5) in the resulting equation, we get the following dimensionless equation for $\psi^{(1)}$

$$E^4\psi^{(1)} = 0, \tag{9}$$

where the second order differential operator E^2 is expressed as

$$E^2 = \frac{\partial^2}{\partial r^2} + \frac{1-\zeta^2}{r^2}\frac{\partial^2}{\partial\zeta^2}, \quad \zeta = \cos\theta. \tag{10}$$

The general solution of (9), which is non-singular everywhere in the flow field, is given as

$$\psi^{(1)} = [a_2 r^2 + b_2 r^{-1} + c_2 r^4 + d_2 r]G_2(\zeta) + [a_3 r^3 + + b_3 r^{-2} + c_3 r^5 + d_3]G_3(\zeta) +$$

$$\sum_{n=4}^{\infty}[A_n r^n + B_n r^{-n+1} + C_n r^{n+2} + D_n r^{-n+3}]G_n(\zeta), \tag{11}$$

where $1 + \alpha_k G_k \leq r \leq 1/\eta$.

While for the fluid flow within the Reiner-Rivlin liquid spheroid by [16], we may take

$$\psi^{(2)} = \psi_0 + \psi_1 S + \psi_2 S^2 + \sum_{n=4}^{\infty}[e_n r^n + f_n r^{n+2}]G_n(\zeta). \tag{12}$$

With the aid of (8), we can now write the relation (12) explicitly in the form:

$$\psi^{(2)}(r,\zeta) = [(e_2 - 2)r^2 + (f_2 + 2)r^4 + \frac{4}{63}S^2 r^6]G_2(\zeta) + [e_3 r^3 + (f_3 + \frac{4}{21}S)r^5]G_3(\zeta) +$$

$$\sum_{n=4}^{\infty}[E_n r^n + F_n r^{n+2}]G_n(\zeta), \tag{13}$$

where $r \leq 1 + \alpha_k G_k$, $\zeta = \cos\theta$, and $G_n(\zeta)$ are the Gegenbauer functions, defined in the book by Abramowitz and Stegun [1], related to the Legendre functions $P_n(\zeta)$ by the relation

$$G_n(\zeta) = \frac{P_{n-1}(\zeta) - P_n(\zeta)}{2n-1}, \quad n \geq 2.$$

Let the equation of the surface S of a spheroid approximating that of the sphere $R = a$, i.e., $r = 1$ in the polar form be $R = a[1 + f(\theta)]$ or $r = 1 + f(\theta)$. The orthogonality relations of Gegenbauer functions permit us, in general, to write $f(\theta)$ in the expanded form as $f(\theta) = \sum_{k=2}^{\infty}\alpha_k G_k(\zeta)$. Hence, we can take the surface S to be of the form

$$r = 1 + \alpha_k G_k(\zeta) \tag{14}$$

and neglect terms of $o(\alpha_k) \geq 2$. In case of Newtonian fluid past a perfect Reiner-Rivlin liquid sphere in spherical container the only coefficients that contribute to $\psi^{(1)}$ and $\psi^{(2)}$ are a_2, b_2, c_2, d_2, e_2, f_2 and f_3 and consequently we expect all other remaining coefficients appearing in the equations (11) and (13) to be of order α_k. Hence, except where the coefficients a_2, b_2, c_2, d_2, e_2, f_2 and f_3 appear, we may take the surface S to be a perfect sphere, i.e., $r = 1$ instead of its approximate form (14).

3. Boundary conditions and determination of arbitrary constants

The arbitrary constants appearing in (11) and (13) to be determined by applying the following the boundary conditions, which are physically realistic and mathematically consistent for the present proposed problem:

(a) The kinematic condition of mutual impenetrability at the interface implies that we may take

$$\psi^{(1)} = 0, \qquad \psi^{(2)} = 0 \qquad \text{on} \quad r = 1 + \alpha_k G_k(\zeta). \tag{15}$$

(b) We assume the continuity of tangential velocity across the interface, hence we have

$$\frac{\partial \psi^{(1)}}{\partial r} = \frac{\partial \psi^{(2)}}{\partial r} \qquad \text{on} \quad r = 1 + \alpha_k G_k(\zeta). \tag{16}$$

(c) We further assume that the presence of interfacial tension only produces a discontinuity in the normal stress τ_{rr} and does not in any way affect tangential stress $\tau_{r\theta}$, i.e., $\tau_{r\theta}^{(1)} = \tau_{r\theta}^{(2)}$ on the surface S of the spheroid which can be shown to be equivalent to

$$\lambda \frac{\partial}{\partial r} \left(\frac{1}{r^2} \frac{\partial \psi^{(1)}}{\partial r} \right) = \frac{\partial}{\partial r} \left(\frac{1}{r^2} \frac{\partial \psi^{(2)}}{\partial r} \right) \qquad \text{on} \quad r = 1 + \alpha_k G_k(\zeta). \tag{17}$$

(d) On the spherical container, the kinematic condition of impenetrability at the surface and the assumption of no slip there lead respectively to

$$\psi^{(1)} = \frac{1}{2} r^2 \sin^2 \theta$$

and

$$\frac{\partial}{\partial r} \left(\psi^{(1)} - \frac{1}{2} r^2 \sin^2 \theta \right) = 0 \quad \text{on} \quad r = \frac{1}{\eta}, \tag{18}$$

where $\lambda = \frac{\mu_1}{\mu_2}$ and $\eta = \frac{a}{b}$. The arbitrary constants encountering in (11) and (13) can be determined from the above boundary conditions, and the results are given in Appendix A. Thus, the stream functions for both the external and internal flow fields are now completely known and given respectively by

$$\psi^{(1)} = [a_2 r^2 + b_2 r^{-1} + c_2 r^4 + d_2 r] G_2(\zeta) + (A_{k-2} r^{k-2} + B_{k-2} r^{-k+3} + C_{k-2} r^k +$$
$$D_{k-2} r^{-k+5}) G_{k-2}(\zeta) + (A_k r^k + B_k r^{-k+1} + C_k r^{k+2} + D_k r^{-k+3}) G_k(\zeta) +$$
$$(A_{k+2} r^{k+2} + B_{k+2} r^{-k-1} + C_{k+2} r^{k+4} + D_{k+2} r^{-k+1}) G_{k+2}(\zeta), \tag{19}$$

$$\psi^{(2)} = \left[(e_2 - 2) r^2 + (f_2 + 2) r^4 + \frac{4}{63} S^2 r^6 \right] G_2(\zeta) + [E_{k-2} r^{k-2} + F_{k-2} r^k] G_{k-2}(\zeta) +$$
$$(E_k r^k + F_k r^{k+1}) G_k(\zeta) + (E_{k+2} r^{k+2} + F_{k+2} r^{k+4}) G_{k+2}(\zeta). \tag{20}$$

Therefore, the Stokes flow past a Reiner-Rivlin liquid spheroid in spherical container is duly determined.
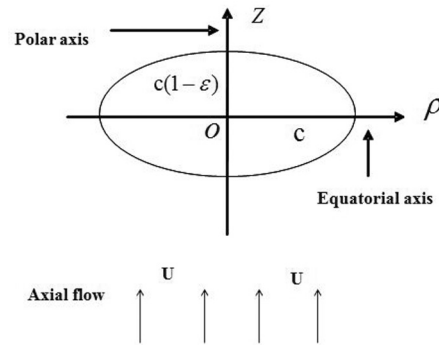
Fig. 2. Oblate spheroid in meridional two dimensional plane

4. Application to a Reiner-Rivlin liquid oblate spheroid

As an application of the foregoing discussion, we now address the particular case of a Reiner-Rivlin liquid oblate spheroid (see Fig. 2) at the instant it passes the centre a spherical container whose equation we take as

$$\frac{x^2 + y^2}{c^2} + \frac{z^2}{c^2(1 - \epsilon)^2} = 1. \tag{21}$$

Therefore, the polar form of the equation (21) to the order $O(\epsilon)$ takes the form

$$R = a[1 + \epsilon G_2(\zeta)] \text{ or } r = 1 + 2\epsilon G_2(\zeta), \tag{22}$$

where $a = c(1 - \epsilon)$. For an oblate fluid spheroid, the results of the previous section can be applied by taking $k = 2, \alpha_k = 2\epsilon$. Therefore, the expressions of stream functions for external and internal flows now get reduced respectively to

$$\psi^{(1)} = [a_2 r^2 + b_2 r^{-1} + c_2 r^4 + d_2 r]G_2(\zeta) + [A_2 r^2 + B_2 r^{-1} + C_2 r^4 + D_2 r]G_2(\zeta) +$$
$$[A_4 r^4 + B_4 r^{-3} + C_4 r^6 + D_4 r^{-1}]G_4(\zeta), \tag{23}$$
$$\psi^{(2)} = \left[(e_2 - 2)r^2 + (f_2 + 2)r^4 + \frac{4}{63}S^2 r^6\right]G_2(\zeta) + (E_2 r^2 + F_2 r^4)G_2(\zeta) +$$
$$(E_4 r^4 + F_4 r^6)G_4(\zeta). \tag{24}$$

5. Evaluation of drag on Reiner-Rivlin liquid oblate spheroid and associated wall effects

Now, for the fluid flow problems in spherical container, one of the most significant physical quantities is the drag force and associated wall effects experienced by the inner non-Newtonian liquid spheroid.

5.1. Drag force (F)

To evaluate the drag force experienced by the inner liquid spheroid in spherical container, we appeal to a simple elegant formula derived by Happel and Brenner [4]

$$F = \mu_1 \pi \int_0^\pi \varpi^3 \frac{\partial}{\partial R}\left(\frac{E^2 \psi_d^{(1)}}{\varpi^2}\right) R \, d\theta, \tag{25}$$

163

where $\varpi = R\sin\theta$ and $\psi_d^{(1)}$ is the dimensional form of stream function defined in (23) and after some working $E^2\psi_d^{(1)}$ simplifies to

$$
\begin{aligned}
E^2\psi_d^{(1)} = Uc^2\sin^2\theta[&40c^2R^5(1+2\epsilon)c_2 - 8c^5R^2(1-\epsilon)d_2 - 8c^5R^2(1-\epsilon)D_2 - \\
&(15c^7 + 25c^7\cos 2\theta)D_4 + 40c^2R^5(1+2\epsilon)C_2 + \\
&(27R^7 + 45R^7\times\cos 2\theta)C_4]/8c^6R^3.
\end{aligned}
\tag{26}
$$

Substituting the value of $E^2\psi_d^{(1)}$ in (25) and carrying out the integration with respect to θ, the dimensional drag simplifies to

$$
F = 4c\pi U(1-\epsilon)(d_2 + D_2)\mu_1.
\tag{27}
$$

5.2. Wall correction factor (K):

The wall correction factor K is defined as the ratio of the actual drag experienced by the liquid spheroid in the enclosure and the drag on a liquid spheroid in an infinite expanse of fluid. With the aid of (27) and (36), this becomes

$$
K = -\frac{(1+\lambda)(1-\epsilon)(d_2+D_2)}{\frac{1}{6}(1-\epsilon)\left(6\lambda + 9 + \frac{32}{63}S^2\right) + \frac{2\epsilon}{945}(567 + 378\lambda + 160S^2)},
\tag{28}
$$

where

$$
d_2 = [2(16S^2(2 - 5\eta^3 + 3\eta^5) + 189(3 + 3\eta^5(-1 + \lambda) + 2\lambda))]\Delta,
\tag{29}
$$

$$
\begin{aligned}
D_2 = (-1+\eta)^2[&8\epsilon(16S^2(-1+\eta)^2(48\eta^7(-1+\lambda) - 40(1+\lambda) - 5\eta^4(-41 + 2\lambda) - \\
&40\eta^3(-1 + 4\lambda) + 20\eta^5(5 + 4\lambda) - 16\eta^2(7 + 13\lambda) - 8\eta(11 + 14\lambda) - \\
&8\eta(11 + 14\lambda) + 3\eta^6(-19 + 34\lambda)) - 189(2 + 4\eta + 6\eta^2 + 3\eta^3)(6 + 10\lambda + \\
&4\lambda^2 + 3\eta^5(3 - 5\lambda + 2\lambda^2) + 5\eta^3(-3 + \lambda + 2\lambda^2)))]\Delta^2/945.
\end{aligned}
\tag{30}
$$

and Δ is given by (A.8). These are respectively the new results for the drag and wall effects on a Reiner-Rivlin liquid spheroid at the instant it passes the center of a spherical envelope.

6. Results and discussion

It is important to consider some limiting situations of the drag force as discussed below:

(i) *A perfect Reiner-Rivlin liquid sphere in spherical container* $(\epsilon \to 0)$:

We get

$$
F = \frac{8c\pi U(16S^2(2 - 5\eta^3 + 3\eta^5) + 189(3 + 3\eta^5(-1 + \lambda) + 2\lambda))\mu_1}{189(-1 + \eta)^3(4\eta^3(-1 + \lambda) + 4(1 + \lambda + \eta^2(-3 + 6\lambda) + \eta(3 + 6\lambda)))},
\tag{31}
$$

a result previously obtained by [16].

(ii) *A perfect Reiner-Rivlin liquid sphere in an unbounded medium* $(\eta \to 0)$:

From (31), when $\eta \to 0$, we get

$$
F = \frac{-2Uc\pi\mu_1(\frac{32}{63}s^2 + 6\lambda + 9)}{3(1+\lambda)},
\tag{32}
$$

where $\lambda = \frac{\mu_1}{\mu_2}$. This result has been obtained previously by [21].

(iii) *Newtonian liquid oblate spheroid in spherical envelope* $(S \to 0)$:

From (27), when $S \to 0$, we get

$$
\begin{aligned}
F = &-8cU(-1+\epsilon)(-1+\eta)^2[4\epsilon(2+4\eta+6\eta^2+3\eta^3)(6+10\lambda+4\lambda^2+ \\
&3\eta^5(3-5\lambda+2\lambda^2)+5\eta^3(-3+\lambda++2\lambda^2))+5(-1+\eta)(12\eta^8(-1+\lambda)^2+ \\
&12\eta^5(-1+\lambda^2)+9\eta^7(1-3\lambda+2\lambda^2)+9\eta^6(-1-\lambda+2\lambda^2)+ \\
&4\eta^3(-3+\lambda+2\lambda^2)+4(3+5\lambda+2\lambda^2)+3\eta^2(-3+4\lambda+4\lambda^2)+ \\
&3\eta(3+8\lambda+4\lambda^2))]\Delta^2\mu_1/5.
\end{aligned}
\tag{33}
$$

This is the new result reported in this paper.

(iv) *Newtonian liquid sphere in spherical envelope* $(\epsilon \to 0)$:

From (33), when $\epsilon \to 0$, we get

$$
F = 1\,512c\pi\mu_1 U[3+3\eta^5(-1+\lambda)+2\lambda]\Delta,
\tag{34}
$$

a well known result reported earlier by [4] and later by [16].

(v) *Newtonian liquid oblate spheroid in unbounded medium* $(\eta \to 0)$:

From (33), when $\eta \to 0$, we get

$$
F = -\frac{6c\pi U\mu_1 \left(1-\frac{1}{5}\epsilon\right)\left(1+\frac{2}{3}\lambda\right)}{1+\lambda}.
\tag{35}
$$

The result was earlier obtained by [22].

(vi) *Reiner-Rivlin liquid oblate spheroid in unbounded medium* $(\eta \to 0)$:

From (27), we have

$$
F = -\frac{4c\pi U\mu_1}{1+\lambda}\left[\frac{(1-\epsilon)\left(6\lambda+9+\frac{32}{63}S^2\right)}{6}+\frac{2\epsilon(567+378\lambda+160S^2)}{945}\right].
\tag{36}
$$

The result was previously obtained by [19].

(vii) *Drag on a Reiner-Rivlin liquid sphere of volume equal to the volume of a Reiner-Rivlin liquid oblate spheroid:*

A perfect Reiner-Rivlin liquid sphere in spherical container of radius equal to $c(1-\epsilon/3)$ will have the volume as oblate spheroid. Therefore, the drag force experienced by a Reiner-Rivlin liquid sphere of radius $c(1-\epsilon/3)$ in spherical container is

$$
F = 8c\pi\left(1-\frac{\epsilon}{3}\right)\mu_1 U[16S^2(2-5\eta^3+3\eta^5)+189(3+3\eta^5(-1+\lambda)+2\lambda)]\Delta.
\tag{37}
$$

On comparison with (27), we make out that a liquid sphere of equal volume experiences a smaller resistance than the liquid oblate spheroid(see Fig. 15).
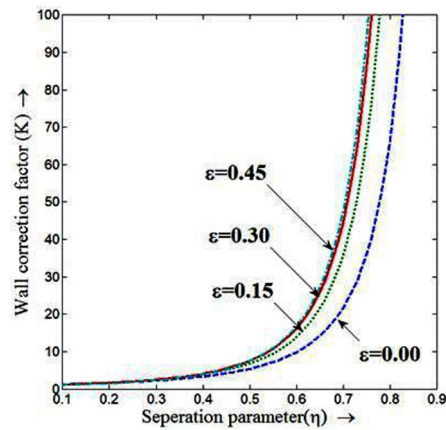
Fig. 3. Variation of the wall correction factor K with η for various values of deformation parameter ϵ at $S = 0.5$ and $\lambda = 0.5$
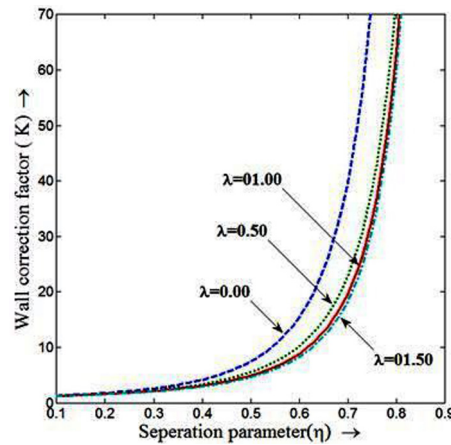

Fig. 4. Variation of the wall correction factor K with η for various values of viscosity ratio λ at $S = 0.5$ and $\epsilon = 0.25$

The effect of the deformation parameter ϵ and separation parameter η on the wall correction factor K has been plotted in Fig. 3 for a fixed value of λ and S. It can be observed from Fig. 3 that the wall correction factor K is increasing with the increasing deformity ($0 \leq \epsilon \leq 0.45$) of the liquid spheroid and separation parameter η. The figure clearly indicates that the wall effects on Reiner-Rivlin liquid sphere is the lowest as compared with such effects on liquid spheroid. The figure also exhibits that the growth rate of the wall correction factors decreases as the deformation of the liquid sphere increases. For ($0.46 \leq \epsilon \leq 0.52$), the wall correction factor K increases almost with the equal amounts for different values of ϵ in the range 0.46 to 0.52 when the separation parameter varies from 0.1 to 0.9. However, for the values of the deformation parameter ϵ greater than 0.5, there is reported a reversal in behavior of the wall correction factor K, i.e., the wall correction factor K decreases as the deformation parameter ϵ increases in the range 0.5 to 1. This bizarre and unexpected variation in wall correction factor K may be possibly due to the expansion and the contraction of the surface area and the volume of the oblate spheroid with decreasing and increasing of measure of the deformity respectively in contact with the fluid in spherical envelope as it is clear from Fig. 15.

The variation of the wall correction factor K against the separation parameter η with continuity of tangential stress for various values of viscosity ratio λ is illustrated in Fig. 4. From the figure, it can be observed that, as η increases, the wall effects on liquid spheroid increases. For
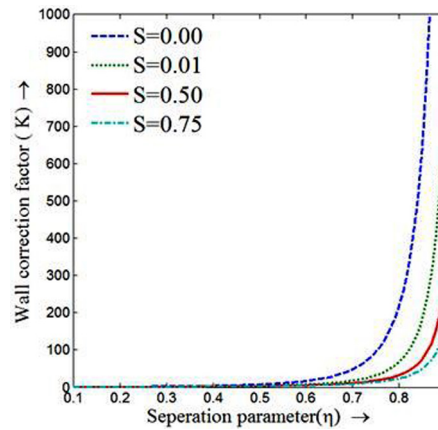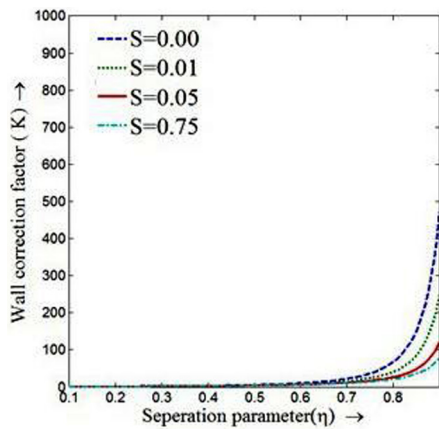
166

Fig. 5. Variation of the wall correction factor K with η for various values of S at $\lambda = 0.5$ and $\epsilon = 0$

Fig. 6. Variation of the wall correction factor K with η for various values of S at $\lambda = 0.5$ and $\epsilon = 0.5$
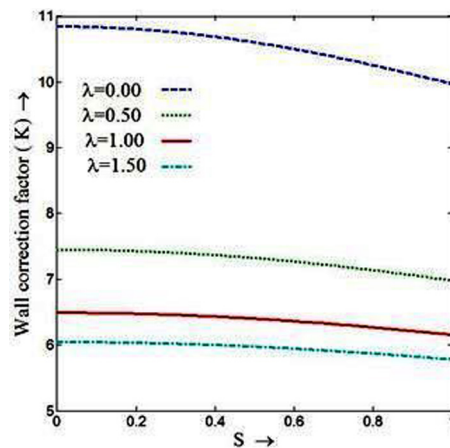

Fig. 7. Variation of the wall correction factor K with S for various values of λ at $\eta = 0.5$ and $\epsilon = 0.5$

smaller values of η, wall correction factor K increases slowly with approximately equal amount for all the values of viscosity ratio λ. But for comparatively larger values of η (> 0.3), K increases very rapidly and differently for different values of λ. Also, the wall correction factor K is decreasing with the increasing viscosity ratio λ. It is interesting to note that for $\lambda > 0.5$, the particle mobility varies slowly with the separation parameter η as compared with the case of lower viscosity ratio.

In Figs. 5 and 6, we have demonstrated the effects of S or the cross viscosity on the wall correction factor K with η for a fixed value of λ and ϵ. It is obvious from the figures that the wall correction factor K is increasing as the separation parameter η is increasing for any fixed S. The wall effects on liquid spheroid is decreasing with increasing S for any η, which is expected. It is also observed from Figs. 5 and 6 that the wall effects on Newtonian liquid spheroid is higher than such effects on Reiner-Rivlin liquid spheroid. In case when $\epsilon = 0$, the results of the present discussion coincide with the results obtained earlier by Ramkissoon and Rahaman [16]. Further, we also conclude from the figures that a perfect liquid sphere experiences less wall effects than a liquid spheroid when both are in spherical container.

We have plotted the wall correction factor K against S ($0 < S < 1$), for various values of viscosity ratio λ in Fig. 7 and for a fixed value of separation parameter η and deformity of the
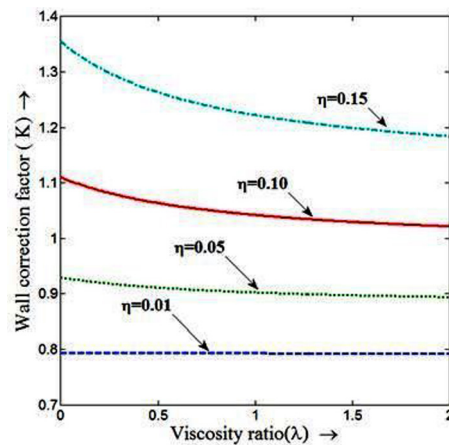
Fig. 8. Variation of the wall correction factor K with λ for various values of η at $S = 0.5$ and $\epsilon = 0.5$
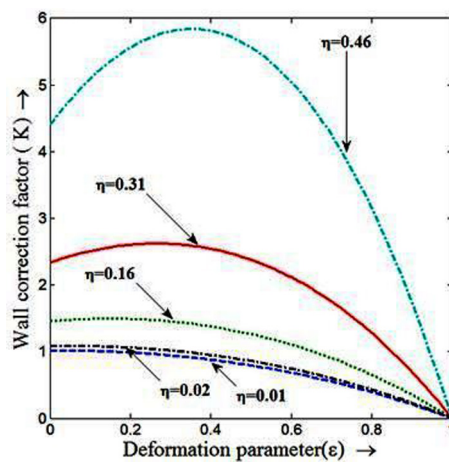

Fig. 9. Variation of the wall correction factor K with deformation parameter ϵ for various values of η at $S = 0.5$ and $\lambda = 0.5$

liquid spheroid ϵ. It can be visualized from the figure that the wall correction factor K, for a fixed λ, decreases with S. We also observe that, for a fixed S, the wall correction factor K shows the identical behavior with λ. It is interesting to note that the wall effects on rigid spheroid is higher than that of a liquid spheroid.

The variation of the wall effects with regard to viscosity ratio λ for various values of separation parameter η is depicted in Fig. 8 for any specified value of S and ϵ. The figure shows that, for relatively large values of separation parameter η, the wall effects on liquid spheroid after a slight decrease becomes almost constant with λ, whereas corresponding to very small values of η, the wall effects on it is almost constant in the entire range of viscosity ratio λ. The graph in Fig. 8 also shows that for a fixed value of λ, the wall effects on liquid spheroid increases with separation parameter η.

The variation of the wall effects on the surface of the Reiner-Rivlin liquid spheroid with deformation parameter ϵ is illustrated in Fig. 9 for numerous values of separation parameter η for a fixed value of S and λ. We can see that corresponding to very small values of η (≤ 0.02), the wall correction factor K is monotonically decreasing function of deformation parameter ϵ. In every other possibility of separation parameter η, wall effects on liquid spheroid first increases
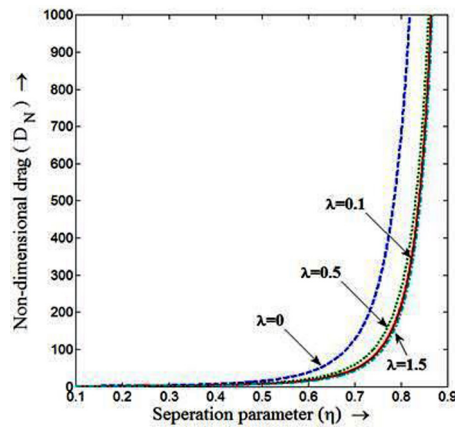
Fig. 10. Variation of the non-dimensional drag D_N with separation parameter η for various values of λ at $S = 0.5$ and $\epsilon = 0.5$
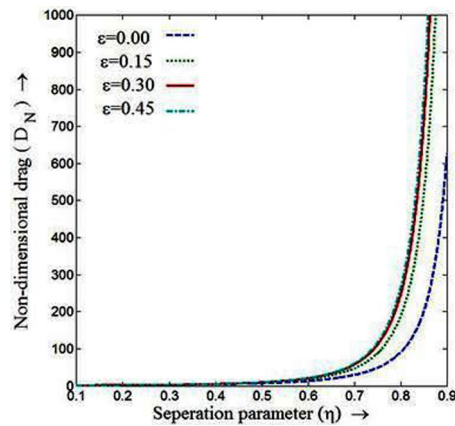

Fig. 11. Variation of the non-dimensional drag D_N with η for various values of deformation parameter ϵ at $S = 0.5$ and $\lambda = 0.5$

and attains to its maximum value at some certain value ϵ and then decreases significantly with the increasing ϵ and vanishes at $\epsilon = 1$. The graph in Fig. 9 also elucidates that the wall effects on liquid spheroid increases as separation parameter η increases for any fixed value of ϵ.

The non-dimensional drag D_N:

$$D_N = \frac{F}{4\pi U c \mu_1} = (1 - \epsilon)(d_2 + D_2). \tag{38}$$

The variation of D_N with respect to the separation parameter η is shown in Fig. 10 for various values of viscosity ratio λ. From the figure, it is observed that as the separation parameter η increases the drag coefficient D_N on Reiner-Rivlin liquid spheroid increases. Also D_N increases as viscosity ratio λ decreases. For relatively smaller values of η, D_N increases slowly with approximately equal amount for all the values of viscosity ratio λ. But for comparatively larger values of η (> 0.5), D_N increases very rapidly and differently with η for different values λ. It is interesting to note that for $\lambda > 1$ drag varies slowly with η as compared with the case of lower viscosity ratio $\lambda < 1$. Further, we also notice that the drag on a rigid spheroid is more than the drag experienced by a Reiner-Rivlin liquid spheroid which is expected.

Fig. 11 illustrates the effects of the deformation parameter ϵ and separation parameter η on the drag D_N for a fixed value of λ and S. It can be observed from Fig. 11 that D_N is increasing
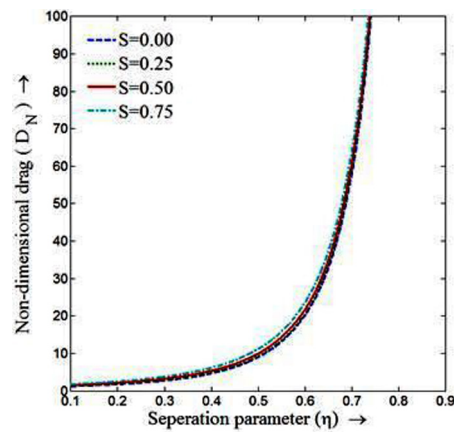
Fig. 12. Variation of the non-dimensional drag D_N with η for various values of S at $\epsilon = 0.5$ and $\lambda = 0.5$
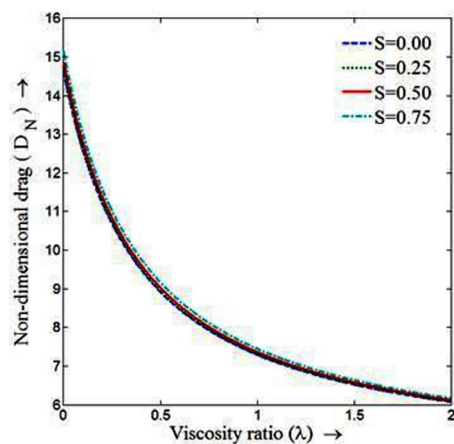

Fig. 13. Variation of the non-dimensional drag D_N with λ for various values of S at $\eta = 0.5$ and $\epsilon = 0.5$

as the separation parameter η is increasing. Also, the drag D_N is increasing with the increasing deformity of the liquid spheroid. The figure evidently indicates that the drag on Reiner-Rivlin liquid sphere is the lowest as compared with dag on the Reiner-Rivlin liquid spheroid. The figure also illustrates that the growth rate of drag D_N keeps on decreasing as the deformation of the liquid sphere is increasing.

We have plotted the drag D_N against η for various values of dimensionless parameter S in Fig. 12 and for a fixed value of deformation parameter ϵ and viscosity ratio λ. It can be seen from the figure that the drag D_N, for a fixed S, increases with η. We also observe that, for a fixed η, the drag D_N shows the identical behavior with S. It is interesting to note that the drag on Newtonian liquid spheroid is the lowest as compared with the drag experienced by a Reiner-Rivlin liquid spheroid.

Fig. 13 exhibits the variation of the drag D_N with λ for various values of dimensionless parameter S for a fixed value of deformation parameter ϵ and separation parameter η. It is observed from Fig. 13 that the drag D_N, for a fixed S, is decreasing with λ. We also observe that, for a fixed λ, the drag D_N is increasing with S. It is interesting to note that the drag on Newtonian liquid spheroid is the lowest as compared with the drag experienced by a Reiner-Rivlin liquid spheroid.

The variation in the drag with S is numerically studied for various values of separation parameter η for a fixed λ and ϵ and presented in Fig. 14 graphically. We observe from the figure that the drag D_N on the Reiner-Rivlin liquid spheroid is increasing with S. Here, the similar
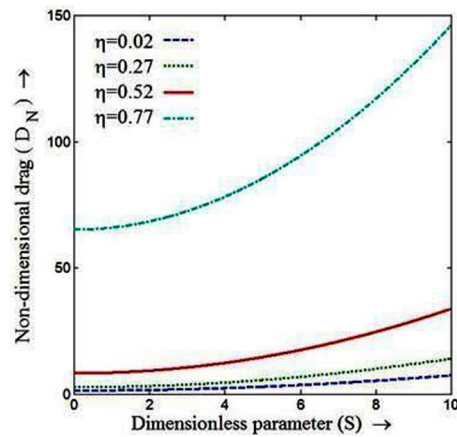
Fig. 14. Variation of the non-dimensional drag D_N with S for various values of separation parameter η at $\lambda = 0.5$ and $\epsilon = 0.01$
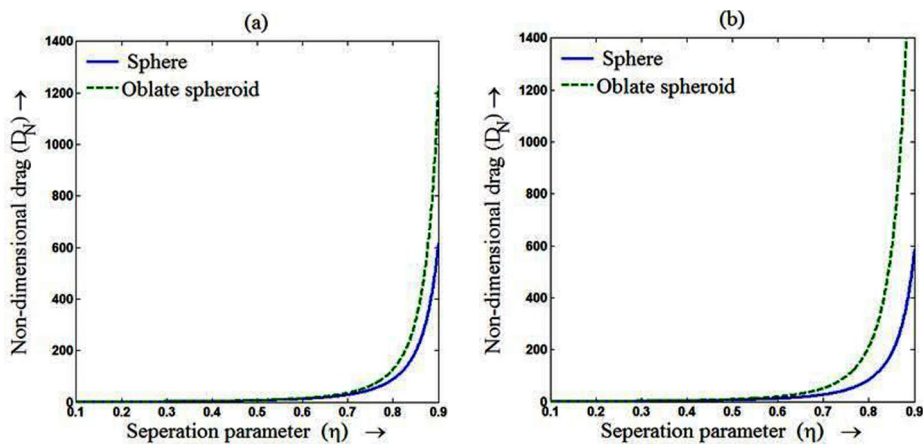

Fig. 15. Variation of the non-dimensional drag with separation parameter η over the sphere and spheroid of equal volumes at $\lambda = 0.5$ and $S = 0.5$ for (a) $\epsilon = 0.05$, (b) $\epsilon = 0.2$

behavior is observed in the variation of the drag on Reiner-Rivlin liquid spheroid with η for a fixed S and the only thing that draws our attention is the growth rate of drag on the body for comparatively lager values of separation parameter is higher than smaller values of η.

A comparative study of drag force experienced by a liquid sphere and a liquid spheroid having equal volumes is performed numerically and corresponding variations are shown graphically in Fig. 15. It can be easily observed that a liquid spheroid of equal volume experiences a larger drag than the liquid sphere. Also, the drag on spheroid increases whereas this drag decreases on sphere with the deformation parameter ϵ.

7. Conclusion

In this paper, an analytical solution to the problem of motion of a Reiner-Rivlin liquid spheroid at the instant it passes the centre of a spherical envelope filled with an incompressible Newtonian fluid is investigated by taking into account the Stokes equation for the external flow, whereas for internal flow expressing the stream function and pressure in a power series of S. An expression for the hydrodynamic drag force D_N on the Reiner-Rivlin liquid spheroid in a spherical shell and wall correction factor K are obtained in closed form in terms of separation parameter η,

cross viscosity, i.e., dimensionless parameter S, viscosity ratio λ and deformation parameter ϵ. It is found that the drag on the liquid spheroid for smaller deformation is more than the drag on a liquid sphere in presence of spherical envelope. But for larger deformation, the behavior is reversed which is physically not possible. Therefore, our proposed model is valid only for small deformation. It is also observed that in case of equal volume and surface area, the drag force exerted on a Reiner-Rivlin liquid spheroid is more than the drag on a liquid sphere. The drag increases with separation parameter η, cross-viscosity μ_c and small deformation parameter ϵ and decreases with viscosity ratio λ. Although the very similar behavior in variation of wall effects on Reiner-Rivlin liquid spheroid is observed, but the cross-viscosity μ_c of Reiner-Rivlin liquid is reported to have a reverse impact on wall effects unlike drag force. Further, it is also observed that wall effects on Newtonian liquid spheroid is found to be more than the such effects on Reiner-Rivlin liquid spheroid and on the other hand the drag force on Newtonian liquid spheroid is found less than the drag on a Reiner-Rivlin liquid spheroid and this drag on liquid spheroid increases with increase in S, i.e., the cross-viscosity. By the analysis of the proposed model and the results obtained here can be easily applied to recover and to collect the information about those liquid bodies whose shape depart a bit from that of a sphere which are suitable for creeping or swift movement through the fluid medium enclosed in an infinite spherical envelope.

References

[1] Abramowitz, M., Stegun, I.A., Handbook of Mathematical Functions, Dover Publications, New York, 1970.

[2] Cunningham, E., On the velocity of steady fall of spherical particles through fluid medium, Proceedings of the Royal Society of London A 83 (1910) 357–365.

[3] Haberman, W.L., Sayre, R.M., Wall effects for rigid and fluid spheres in slow motion with a moving liquid, David Taylor model, Basin Report No. 1143, Washington DC, 1958.

[4] Happel, J., Brenner, H., Low Reynolds Number Hydrodynamics, Prentice-Hall, Engle-wood Cliffs, N. J., 1965.

[5] Iyengar, T.K.V., Srinivasacharya, D., Stokes flow of an incompressible micropolar fluid past an approximate sphere, International Journal of Engineering Science 31 (1) (1993) 115–123.

[6] Jaiswal, B.R., Gupta, B.R., Drag on Reiner-Rivlin liquid sphere placed in a micropolar fluid with non-zero boundary condition for microrotations, International Journal of Applied Mathematics and Mechanics 10 (7) (2014) 93–103.

[7] Jones, R.B., Dynamics of a colloid in a spherical cavity, Theoretical Methods for Micro Scale Viscous Flows, eds. Francois Feuillebois and Antoine Sellier, Transworld Research Network, 2009.

[8] Keh, H.J., Chou, J., Creeping motion of a composite sphere in a concentric spherical cavity, Chemical Engineering Science 59 (2) (2004) 407–415.

[9] Keh, H.J., Lu, Y.S., Creeping motions of a porous spherical shell in a concentric spherical cavity, Journal of Fluids and Structures 20 (5) (2005) 735–747.

[10] Kim, S., Karrila, S.J., Micro hydrodynamics: Principles and Selected Applications, Butterworth-Heinemann, Boston, MA, USA, 1991.

[11] Maul, C., Kim, S., Image of a point force in a spherical container and its connection to the Lorentz reflection formula, Journal of Engineering Mathematics 30 (1–2) (1996) 119–130.

[12] Maul, C., Kim, S., Image systems for a Stokeslet inside a rigid spherical container, Physics of Fluids 6 (6) (1994) 2221–2223.

[13] Oseen, C.W., Hydrodynamik, Akademische Verlagsgesellschaft, Leipzig, 1927.

[14] Palaniappan, D., Creeping flow about a slightly deformed sphere, Zeitschrift für Angewandte Mathematik und Physik 45 (1) (1994) 323–338.

[15] Ramkissoon, H., Majumadar, S.R., Micropolar fluid past a slightly deformed fluid sphere, Zeitschrift für Angewandte Mathematik und Mechanik 68 (3) (1988) 155–160.

[16] Ramkissoon, H., Rahaman, K., Non-Newtonian fluid sphere in a spherical container, Acta Mechanica 149 (1–44) (2001) 239–245.

[17] Ramkissoon, H., Rahaman, K., Wall effects on a spherical particle, International Journal of Engineering Science 41 (3–5) (2003) 283–290.

[18] Ramkissoon, H., Rahaman, K., Wall effects with slip, Zeitschrift für Angewandte Mathematik und Mechanik 83 (11) (2003) 773–778.

[19] Ramkissoon, H., Stokes flow past a non-Newtonian fluid spheroid, Zeitschrift für Angewandte Mathematik und Mechanik 78 (1) (1998) 61–66.

[20] Ramkissoon, H., Polar flow past a Reiner-Rivlin liquid sphere, Journal of Mathematical Sciences 10 (2) (1999) 63–68.

[21] Ramkissoon, H., Stokes flow past a Reiner-Rivlin fluid sphere, Zeitschrift für Angewandte Mathematik und Mechanik 69 (8) (1989) 259–261.

[22] Ramkissoon, H., Stokes flow past a slightly deformed fluid sphere, Journal of Applied Mathematics and Physics 37 (6) (1986) 859–866.

[23] Saad, E.I., Motion of a spheroidal particle in a micropolar fluid contained in a spherical envelope, Canadian Journal of Physics 86 (2008) 1039–1056.

[24] Saad, E.I., Translation and rotation of a porous spheroid in a spheroidal container, Canadian Journal of Physics 88 (2010) 689–700.

[25] Srinivasacharya, D., Krishna Prasad, M., Axi-symmetric motion of a porous approximate sphere in an approximate spherical container, Archives of Mechanics 65 (6) (2013) 485–509.

[26] Srinivasacharya, D., Krishna Prasad, M., Creeping motion of a porous approximate sphere with an impermeable core in spherical container, European Journal of Mechanics B-Fluids 36 (2012) 104–114.

[27] Srinivasacharya, D., Krishna Prasad, M., On the motion of a porous spherical shell in a bounded medium, Advances in Theoretical and Applied Mechanics 5 (6) (2012) 247–256.

[28] Srinivasacharya, D., Krishna Prasad, M., Slow steady rotation of a porous sphere in a spherical container, Journal of Porous Media 15 (12) (2012) 1 105–1 110.

[29] Srinivasacharya, D., Krishna Prasad, M., Steady rotation of a composite sphere in a concentric spherical cavity, Acta Mechanica Sinica 28 (3) (2012) 653–658.

[30] Srinivasacharya, D., Motion of a porous sphere in a spherical container, Compte Rendus Mécanique 333 (8) (2005) 612–616.

[31] Stokes, G. G., On the effect of the internal friction of fluid on the motion of pendulums, Transactions of the Cambridge Philosophical Society 9 (1851) 8–106.

[32] Williams, W.E., On the motion of a sphere in a viscous fluid, Philosophical Magazine 29 (1915) 526–550.

Appendix A

The unknowns appearing in (11) and (13) can be deduced by substituting these equations into the boundary conditions (15)–(18), which lead to the following system of algebraic equations:

$$(a_2 + b_2 + c_2 + d_2)G_2(\zeta) + (2a_2 - b_2 + 4c_2 + d_2)\alpha_k G_k(\zeta)G_2(\zeta) +$$
$$(a_3 + b_3 + c_3 + d_3)G_3(\zeta) + \sum_{n=4}^{\infty}(A_n + B_n + C_n + D_n)G_n(\zeta) = 0, \qquad (A.1)$$

$$\left(e_2 + f_2 + \frac{4}{63}S^2\right)G_2(\zeta) + \left(2e_2 + 4f_2 + 4 + \frac{8}{21}S^2\right)\alpha_k G_k(\zeta)G_2(\zeta)+$$

$$(e_3 + f_3 + \frac{4}{21}S)G_3(\zeta) + 5\left(f_3 + \frac{4}{21}S\right)\alpha_k G_k(\zeta)G_3(\zeta) + \sum_{n=4}^{\infty}(E_n + F_n)G_n(\zeta) = 0, \quad \text{(A.2)}$$

$$\left(2a_2 - b_2 + 4c_2 + d_2 - 2e_2 - 4f_2 - 4 - \frac{8}{21}S^2\right)G_2(\zeta)+$$

$$(2a_2 + 2b_2 + 12c_2 - 2e_2 - 12f_2 - 20 - \frac{40}{21}S^2)\alpha_k G_k(\zeta)G_2(\zeta)+$$

$$\left(3a_3 - 2b_3 + 5c_3 - 3e_3 - 5f_3 - \frac{20}{21}S\right)G_3(\zeta)-$$

$$20\left(f_3 + \frac{4}{21}S\right)\alpha_k G_k(\zeta)G_3(\zeta)+$$

$$\sum_{n=4}^{\infty}[nA_n - (n-1)B_n + (n+2)C_n + (-n+3)D_n - nE_n - (n+2)F_n]G_n(\zeta) = 0, \quad \text{(A.3)}$$

$$[\lambda(-2a_2 + 4b_2 + 4c_2 - 2d_2) + 2e_2 - 4f_2 - 12 - \frac{8}{7}S^2]G_2(\zeta)+$$

$$[\lambda(4a_2 - 20b_2 + 6d_2) - 4e_2 + 8 - \frac{16}{7}S^2]\alpha_k G_k(\zeta)G_2(\zeta)+$$

$$\left[\lambda(10b_3 - 10c_3) - 10\left(f_3 + \frac{4}{21}S\right)\right] \times G_3(\zeta) - 10\left(f_3 + \frac{4}{21}S\right)\alpha_k G_k(\zeta)G_3(\zeta)+$$

$$\sum_{n=4}^{\infty}[\lambda(n(n-3)A_n + (n+2)(n-1)B_n + (n-1)(n+2)C_n + n(n-3)D_n)-$$

$$n(n-3)E_n - (n-1)(n+2)F_n]G_n(\zeta) = 0, \text{(A.4)}$$

$$\left(\frac{a_2 - 1}{\eta^2} + \eta b_2 + \frac{c_2}{\eta^4} + \frac{d_2}{\eta}\right)G_2(\zeta) + \left(\frac{a_3}{\eta^3} + \eta^2 b_3 + \frac{c_3}{\eta^5} + d_3\right)G_3(\zeta)+$$

$$\sum_{n=4}^{\infty}\left(\frac{A_n}{\eta^n} + \frac{B_n}{\eta^{-n+1}} + \frac{C_n}{\eta^{n+2}} + \frac{D_n}{\eta^{-n+3}}\right)G_n(\zeta) = 0 \quad \text{(A.5)}$$

and

$$\left(\frac{2(a_2 - 1)}{\eta} - \eta^2 b_2 + \frac{4c_2}{\eta^3} + d_2\right)G_2(\zeta) + \left(\frac{3a_3}{\eta^2} - 2\eta^3 b_3 + \frac{5c_3}{\eta^4}\right)G_3(\zeta)+$$

$$\sum_{n=4}^{\infty}\left(\frac{nA_n}{\eta^{n-1}} + \frac{(-n+1)B_n}{\eta^{-n}} + \frac{(n+2)C_n}{\eta^{n+1}} + \frac{(-n+3)D_n}{\eta^{-n+2}}\right)G_n(\zeta) = 0. \quad \text{(A.6)}$$

The leading terms, i.e., the coefficients of $G_2(\zeta)$ and $G_3(\zeta)$ in the above system of equations (A.1)–(A.6) must vanish, i.e.,

$$a_2 + b_2 + c_2 + d_2 = 0, \quad 3 + b_3 + c_3 + d_3 = 0, \quad e_2 + f_2 + \frac{4}{63}S^2 = 0, \quad e_3 + f_3 + \frac{4}{21}S = 0,$$

$$2a_2 - b_2 + 4c_2 + d_2 - 2e_2 - 4f_2 - 4 - \frac{8}{21}S^2 = 0, \quad 3a_3 - 2b_3 + 5c_3 - 3e_3 - 5f_3 - \frac{20}{21}S = 0,$$

$$\lambda(-2a_2 + 4b_2 + 4c_2 - 2d_2) + 2e_2 - 4f_2 - 12 - \frac{8}{7}S^2 = 0, \quad \lambda(b_3 - c_3) - f_3 - \frac{4}{21}S = 0,$$

$$\eta^2 a_2 + \eta^5 b_2 + c_2 + \eta^3 d_2 - \eta^2 = 0, \quad \eta^3 a_3 + \eta^7 b_3 + c_3 + \eta^5 d_3 = 0,$$
$$2\eta^2 a_2 - \eta^5 b_2 + 4c_2 + \eta^3 d_2 - 2\eta^2 = 0, \quad 3\eta^2 a_3 - 2\eta^7 b_3 + 5c_3 = 0. \tag{A.7}$$

Solving (A.7) yields

$$a_3 = 0, \quad b_3 = 0, \quad c_3 = 0, \quad d_3 = 0, \quad e_3 = 0, \quad f_3 = -\frac{4}{21}S,$$
$$e_2 = [4S^2(42\eta^2 + \eta(7 - 6\lambda) + 4\eta^4(-7 + 3\lambda) - 4(7 + 3\lambda) + \eta^3(7 + 6\lambda)) +$$
$$189(-8 + 2\eta + 8\eta^4(-1 + \lambda) - 6\lambda + 6\eta^2(2 + \lambda) + \eta^3(2 + 7\lambda))]\Delta,$$
$$f_2 = -[8S^2(30\eta^2 + \eta(5 - 6\lambda) + 4\eta^4(-5 + 3\lambda) - 4(5 + 3\lambda) + \eta^3(5 + 6\lambda)) +$$
$$189(-8 + 2\eta + 8\eta^4(-1 + \lambda) - 6\lambda + 6\eta^2(2 + \lambda) + \eta^3(2 + 7\lambda))]\Delta,$$
$$a_2 = -[32S^2(3\eta - 5\eta^3 + 2\eta^6) + 189(5\eta^3 + 4(1 + \lambda) + \eta^5(-9 + 6\lambda))]\Delta,$$
$$b_2 = -[32S^2(2 - 3\eta + \eta^3) + 378(1 + \eta^3(-1 + \lambda))]\Delta,$$
$$c_2 = [\eta^3(32S^2(-1 + \eta)^2(1 + 2\eta) + 189(3 - 3\eta^2 + 2\lambda))]\Delta,$$
$$d_2 = [2(16S^2(2 - 5\eta^3 + 3\eta^5) + 189(3 + 3\eta^5(-1 + \lambda) + 2\lambda))]\Delta, \tag{A.8}$$

where

$$\frac{1}{\Delta} = 189(-1 + \eta)^3[4\eta^3(-1 + \lambda) + 4(1 + \lambda) + \eta^2(-3 + 6\lambda) + \eta(3 + 6\lambda)].$$

By using these values, the equations (A.1)–(A.6) now get reduced respectively to

$$\xi_1 \alpha_k G_k(\zeta) G_2(\zeta) + \sum_{n=4}^{\infty} (A_n + B_n + C_n + D_n) G_n(\zeta) = 0, \tag{A.9}$$

$$\xi_2 \alpha_k G_k(\zeta) G_2(\zeta) + \sum_{n=4}^{\infty} (E_n + F_n) G_n(\zeta) = 0, \tag{A.10}$$

$$\xi_4 \alpha_k G_k(\zeta) G_2(\zeta) + \sum_{n=4}^{\infty} [nA_n + (-n + 1)B_n + (n + 2)C_n +$$
$$(-n + 3)D_n - nE_n - (n + 2)F_n]G_n(\zeta) = 0, \tag{A.11}$$

$$\xi_6 \alpha_k G_k(\zeta) G_2(\zeta) + \sum_{n=4}^{\infty} [\lambda(n(n - 3)A_n + (n + 2)(n - 1)B_n +$$
$$(n - 1)(n + +2)C_n + n(n - 3)D_n) - n(n - 3)E_n - (n - 1)(n + 2)F_n]G_n(\zeta) = 0, \tag{A.12}$$

$$\sum_{n=4}^{\infty} \left(\frac{A_n}{\eta^n} + \frac{B_n}{\eta^{-n+1}} + \frac{C_n}{\eta^{n+2}} + \frac{D_n}{\eta^{-n+3}} \right) G_n(\zeta) = 0, \tag{A.13}$$

$$\sum_{n=4}^{\infty} \left(\frac{nA_n}{\eta^{n-1}} + \frac{(-n + 1)B_n}{\eta^{-n}} + \frac{(n + 2)C_n}{\eta^{n+1}} + \frac{(-n + 3)D_n}{\eta^{-n+2}} \right) G_n(\zeta) = 0, \tag{A.14}$$

where

$$\xi_1 = \xi_2 = [2(16S^2(-1+\eta)^2(4+7\eta+4\eta^2) - 189(2+4\eta+6\eta^2+3\eta^3)\lambda)]\Lambda,$$
$$\xi_4 = -3[2(-189(2+4\eta+6\eta^2+3\eta^3) + 32S^2(-2-\eta+\eta^3+2\eta^4))(-1+\lambda)]\Lambda,$$
$$\xi_6 = -[4(-189\lambda(13+10\eta0^3(-1+\lambda)+3\eta^5(-1+\lambda)+2\lambda)+8S^2(68\eta^6(-1+\lambda) - 10\eta^3(17+\lambda) - 9\eta^5(-17+12\lambda) + 9\eta(17+18\lambda) - 4(17+28\lambda)))]\Lambda$$

and

$$\frac{1}{\Lambda} = 189(-1+\eta)[4\eta^3(-1+\lambda)+4(1+\lambda)+\eta^2(-3+6\lambda)+\eta(3+6\lambda).$$

To determine the remaining arbitrary constants in equations (A.9)–(A.14), we use the following identity

$$G_k G_2 = -\frac{(k-2)(k-3)}{2(2k-1)(2k-3)}G_{k-2} + \frac{k(k-1)}{(2k+1)(2k-3)}G_k -$$
$$\frac{(k+1)(k+2)}{2(2k-1)(2k+1)}G_{k+2}, \qquad k \geq 2. \tag{A.15}$$

In solving the system of equations (A.9)–(A.14), we glimpse that $A_n = B_n = C_n = D_n = E_n = F_n = 0$, if $n \neq k-2, k, k+2$ and when $n = k-2, k, k+2$, we have the following system of equations:

$$\xi_1\alpha_k\phi_n + A_n + B_n + C_n + D_n = 0, \tag{A.16}$$
$$\xi_2\alpha_k\phi_n + E_n + F_n = 0, \tag{A.17}$$
$$\xi_4\alpha_k\phi_n + nA_n - (n-1)B_n + (n+2)C_n - (n-3)D_n - nE_n - (n+2)F_n = 0, \tag{A.18}$$
$$\xi_6\alpha_k\phi_n + \lambda[n(n-3)A_n + (n+2)(n-1)B_n + (n-1)(n+2)C_n + n(n-3)D_n] - n(n-3)E_n - (n-1)(n+2)F_n = 0, \tag{A.19}$$
$$\frac{A_n}{\eta^n} + \frac{B_n}{\eta^{-n+1}} + \frac{C_n}{\eta^{n+2}} + \frac{D_n}{\eta^{-n+3}} = 0, \tag{A.20}$$
$$\frac{nA_n}{\eta^{n-1}} + \frac{(-n+1)B_n}{\eta^{-n}} + \frac{(n+2)C_n}{\eta^{n+1}} + \frac{(-n+3)D_n}{\eta^{-n+2}} = 0, \tag{A.21}$$

where

$$\phi_{k-2} = -\frac{(k-2)(k-3)}{2(2k-1)(2k-3)}, \quad \phi_k = \frac{k(k-1)}{(2k+1)(2k-3)}, \quad \phi_{k+2} = -\frac{(k+1)(k+2)}{2(2k-1)(2k+1)}.$$

The solutions of the equations (A.16)–(A.21) yield the expressions for A_n, B_n, C_n, D_n, E_n, and F_n when $n = k-2, k, k+2$.